Robust Terrain-Aided Navigation through Sensor Fusion

Lager, Mårten; Topp, Elin Anna; Malec, Jacek

Published in:
23rd International Conference on Information Fusion Virtual Conference

DOI:
10.23919/FUSION45008.2020.9190578

2020

Document Version:
Publisher's PDF, also known as Version of record

Robust Terrain-Aided Navigation through Sensor Fusion

Mårten Lager
Department of Computer Science
Lund University
Saab Kockums AB
Lund, Sweden
marten.lager@cs.lth.se

Elin A. Topp
Department of Computer Science
Lund University
Lund, Sweden
elin_anna.topp@cs.lth.se

Jacek Malec
Department of Computer Science
Lund University
Lund, Sweden
jacek.malec@cs.lth.se

***Abstract*—To make autonomous, affordable ships feasible in the real world, they must be capable of safely navigating without fully relying on GPS, high-resolution 3D maps, or high-performance navigation sensors. We suggest a method for estimating the position using affordable navigation sensors (compass and speed log or inertial navigation sensor), sensors used for perception of the environment (cameras, echo sounder, magnetometer), and publicly available maps (sea charts and magnetic intensity anomalies maps). A real-world field trial has shown that the proposed fusion mechanism provides accurate and robust navigation, applicable for affordable autonomous ships.**

***Index Terms*—Localization, Unmanned Surface Vessel, Autonomous System, Particle Filter, Terrain Navigation**

I. Introduction

Unmanned autonomous ships (surface and sub-surface) face challenges when it comes to navigating safely at sea. Today mainly Global Navigation Satellite Systems (GNSS) are used, where the Global Positioning System (GPS) is the most common one. As GNSS systems easily can be jammed or even spoofed [2], and do not work if submerged or objects are blocking the path towards the satellites, it is essential to complement the navigation ability with other solutions. Human operators typically do this by comparing the surrounding world to the digital sea chart, as well as by watching out for surrounding obstacles as a lookout, see Fig. 1. Humans are skilled in having a good overview of the navigation, and can reason about and adapt to the situation if the surrounding area does not match what is seen in the sea chart. The reasoning comes at a cognitive cost, though, and after a while, a human loses focus with increased risks for mistakes [3]. This is one of the reasons why 90–95% of all collision accidents at sea since 1999 are caused by human errors [4].

To surpass the human's ability to navigate, a machine should use the strength it possesses, instead of mimicking how humans navigate. We believe a good approach should use several data sources weighted according to performance and combine them to generate the best statistical position estimation.

This work was partially supported by the Wallenberg AI, Autonomous Systems and Software Program (WASP) [1]. Saab Kockums provided the ship used for data gathering.

Fig. 1. The main author is acting as a lookout during the field trial.

In previous work, we presented Terrain-Aided Navigation (TAN) and evaluated the performance of a Particle Filter (PF)-based approach using simulated data only [5]. It used a high-performance INS and compared standard map data with fused data from depth, magnetic field intensity, intersection of those, and the dead reckoned position. We have used that earlier work as a baseline for our new approach presented in this paper. Here, we have refined the approach by using, instead of the high-performance INS, affordable sensors such as compass and log. We have also extended the underlying algorithm to use Kalman Filter (KF) feedback, as well as bearings to landmarks. Instead of evaluating the performance using simulated data, we have collected data in a real-world field trial in the Swedish Archipelago.

With this, we are able to combine and evaluate standard technologies regarding their applicability in affordable ships in a real-world scenario that can use data from publicly available maps (e.g., sea charts) and still perform sufficiently well.

Using the collected data, we have created a simulator with a GUI, see Fig. 2, where we have evaluated our algorithm using different fusion mixes while having various amounts of simulated drift. Our evaluations show that the performance, especially regarding the robustness of the system, is increased, when combining multiple data sources.

Summarising, our main contributions are:

- a robust approach where we conduct TAN based on fused data,
- a thorough evaluation of the approach on real-world data,
- evidence of the applicability of affordable sensors for

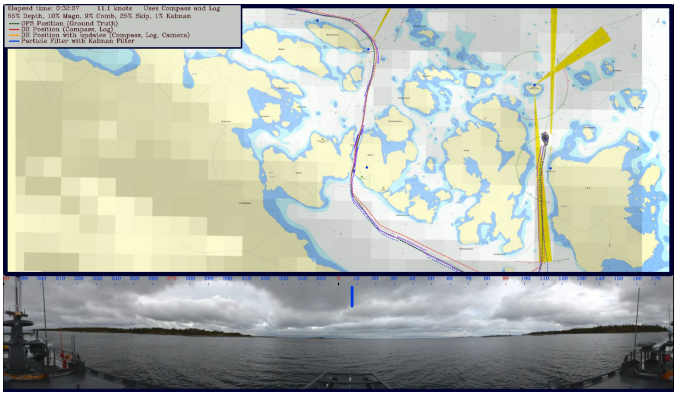

Fig. 2. Screenshot of the GUI. At the bottom is the 360°-video presented, wherein this case the ship has course 7°. The top part is showing the sea chart, and the current route, where the ship and surrounding particles currently are to the right in the image. The overlayed magnetic intensity anomalies map is seen as squares in various greyscale.

reasonable results, instead of high-accuracy sensors,
- evidence of the applicability of regular sea charts and publicly available magnetic intensity anomaly maps, instead of high-resolution 3D terrain maps.

The paper is organized as follows. In Section II, related work is described regarding how bottom depth and magnetic intensity have been used by PFs to implement TAN. Section III describes the algorithm and how the maps are interpreted, followed by Section IV that describes the sensors that have been used on the boat. The tests are described in Section V, with the Conclusion in Section VI.

II. Related Work

We discuss in the following related work based on TAN using different types of sensory data available at sea.

A. Particle Filter using Depth Data

Our approach to TAN uses bottom depth measurements and compares these with a known map. Because it uses distributions that are highly nonlinear, non-Gaussian, and multimodal, classical methods with low computer power needs, such as KF perform poorly [6]. By this, KF implementations, which were more common before the year 2000, have nowadays mainly been replaced by implementations of PFs and Point Mass Filters (PMF) [7]. We apply the multi-hypothesis filtering method PF, with the ability to tackle the mentioned difficulties [8], [9].

It has been shown many times that a PF can estimate the position by comparing the bottom depth with a known high-resolution 3D-terrain map [8]–[15]. Many of these references focus on a use-case for Autonomous Underwater Vehicles (AUV) [9]–[15], where it is of particular importance to be able to navigate without a GNSS system. An AUV is typically equipped with a multibeam sonar in order to map the seabed, and as the equipment is already available, it has also been used for the PF [9]–[13]. We use a single-beam echosounder instead, which makes the use-case relevant for a more substantial portion of ships.

There are still problems to be solved in order to make the technique applicable to most real-world scenarios. The first problem is that there are almost no areas in the world with high-resolution 3D terrain maps. Because of this, AUV deployments are typically preceded by a ship-based multibeam bathymetry survey of the operating area, followed by processing of the data (outliers are removed), and the construction of the gridded bathymetric reference map [16]. This puts a considerable limitation to the usage of the TAN technology. Hence we instead restrict ourselves only to use publicly available sea charts, which cover most coastlines.

The performance of the PF also increases with varied terrain, but in some areas, the terrain is quite flat, resulting in poor accuracy [17]–[19]. In symmetric terrain, there can also be a problem with sample impoverishment, which can occur when the particle cloud is divided to follow paths that give similar measurement values. Teixeira et al. reduce this problem by using three different types of PFs to different terrains types [14]. Another difficulty that generally is not mitigated is that a PF is vulnerable to outliers in the maps or depth measurements. Peng et al. point out that these outliers can occur in many ways, and they describe how to alleviate the effect by using the Huber function when setting the importance weights for the PF [9].

To mitigate all these types of problems in our work, we do not rely on depth measurements alone, but instead, use a combination of different measurements. By relying on multiple domains, we make our algorithm less susceptible to sample impoverishment and to outliers.

B. Particle Filter using Magnetic Intensity

A magnetic field surrounds Earth, where each ferromagnetic element disturbs this field. These disturbances can for indoor environments be even greater than the natural magnetic field of Earth [20]. For indoor environments, numerous ferromagnetic elements create a complex magnetic field where the magnetic vector varies greatly depending on the location. As long as no major furniture or iron walls are moved, the magnetic field is also quite stable. Frassl et al. use a PF combining the magnetic field with a magnetic anomaly map together with odometry, to localize a mobile robot [21]. In [20] the position of a human user is estimated by measuring the magnetic field and acceleration by only using cheap smartphone sensors.

In our approach, we use the magnetic intensity as a second input to the PF, together with the previously mentioned depth measurements. The magnetic field does not fluctuate nearly as much as for indoor use, and each pixel in the available map corresponds to 185x185m^2. Still, this is enough to improve performance.

C. Using other data for the Particle Filter

Other measurements than depth and magnetic field intensity have been used in research to support a PF. Karlsson et al. used Radar to measure bearings and ranges to land objects [8]. Some echosounder systems measure not only the bottom depth, but also the range to different sediment layers below the

bottom. The benefit of using lower layers of the bottom is that these layers tend to have more variations [17]. The downside is that there are few maps available.

It is also possible to compare the current gravity with a gravity anomaly map, which Musso et al. show can be beneficial for navigation [22]. Other candidates that can be used together with a PF are:

- Celestial Navigation, where, e.g., a star in a specific direction, is present or not [8],
- Bearings to landmarks from, e.g., visual sensors [8].

We have used bearings to landmarks in our project as a third data source to increase the robustness and the performance of the system.

III. Terrain-Aided Navigation with a Mixture Re-sampling Step for Increased Robustness

In the following, we explain our PF based algorithm, and how it has been extended with a mixture function for the re-sampling step, fed by data from depth, magnetic field intensity, and bearings to known landmarks.

A. Transition Model

The ship goes on a surface route, where its state is estimated with N particles, with ($\mathbf{X}_t$) denoting all the N particles in time t yielding:

$$\mathbf{X}_t = \{x_t^{(1)}, x_t^{(2)}, ..., x_t^{(N)}\} \tag{1}$$

Each particle contains the state representation according to:

$$x_t^{(p)} = [\lambda_t^{(p)} \quad \Phi_t^{(p)}]^T \tag{2}$$

where $\lambda_t^{(p)}$ is the latitude of the position for particle p in time t, and $\Phi_t^{(p)}$ is the longitude for the same particle.

At the beginning of each test, N particles are initialized around an initial, known position (x_0) using (3), where the superscript states the particle index and the subscript the time.

$$x_0^p = x_0 + \mathcal{N}(0,\, \sigma^2) : p = 1, 2, ..., N \tag{3}$$

The state changes over time, with the discrete sample time Δ, and is modeled by:

$$x_{t+1} = f(x_t, u_t, \eta_t) = \begin{pmatrix} \lambda_t + v_t \Delta \sin(\varphi_t) \\ \Phi_t + v_t \Delta \cos(\varphi_t) \end{pmatrix} + \eta_t \tag{4}$$

where $u_t = (v_t, \varphi_t)^T$ is the input signal, which consists of the speed v_t and the compass angle φ_t. The η_t is the process noise.

We now have the model to go from one state to the next state. For the particle filter to work, information about how the measured values depth and magnetic intensity y_t depend on the state x_t is also needed. For this, we use the sea chart and the magnetic intensity anomalies map.

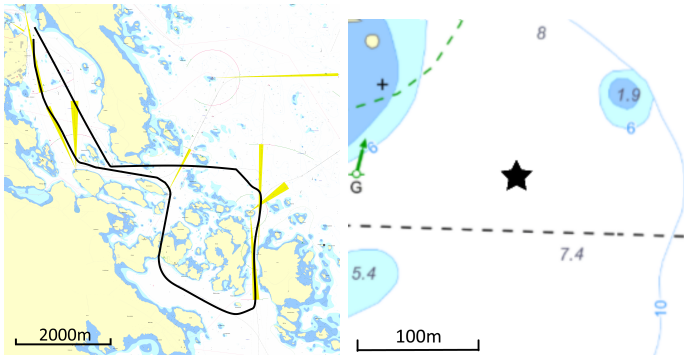

Fig. 3. The left image shows a sea chart over an area outside Västervik in Sweden. The route of the field trial is drawn in black. The right image shows an enlargement of a specific part of the map. The 6m bottom depth line indicates that it is at least 6m deep by the star. The 10m bottom depth line indicates that it is at least 10m deep to the right of the bottom depth line, but does not indicate anything to the location of the star. We have used the bottom depth lines, together with the bottom depth indicators (7.4, 1.9, 8, 5.4) for the creation of a PDF of the bottom depth.

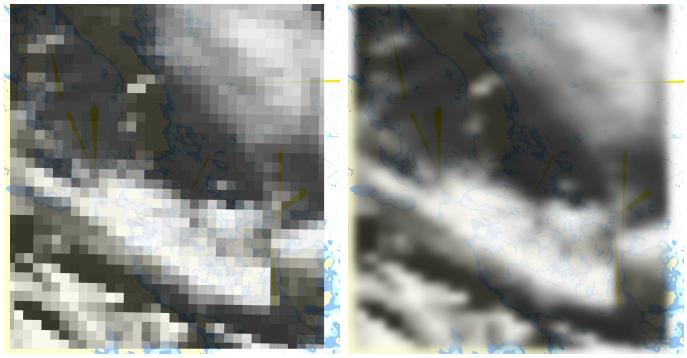

Fig. 4. The magnetic intensity anomalies map is overlayed over the sea chart. From the original map, each pixel has the size of 185x185m^2, see the left image. To get a map that better corresponds to the real world, this low resolution map has been interpolated into a high resolution map, see the right image.

B. Maps

As we use a standard sea chart (see Fig. 3) and a low-resolution magnetic intensity anomalies map (see left part of Fig. 4), it is not possible to look up the depth and magnetic intensity value directly in the location of one particle. Instead, for each particle, we create a Probability Density Functions (PDF) of the depth and the magnetic intensity estimation.

For creating the PDF^{depth}, we gather the bottom depth indicators closest to the specific particle from the sea chart. For the right part of Fig. 3, where the location of a particle is indicated with a star, these are $\{7.4,\ 1.9,\ 8,\ 5.4\}$. We then weight these indicators according to $weight = distance^{-1}$. From these values, we calculate a weighted mean and a weighted standard deviation, which we use for creating the PDF with a normal distribution. The 6m bottom depth line in the right part of Fig. 3 specifies that the minimum bottom depth by the star is 6m, hence the PDF is truncated below 6.0m. The 10m bottom depth, on the other hand, does not provide any more information for the PDF, as the bottom depth

is allowed to be more than 10.0m.

The left part of Fig. 4 shows a publicly available magnetic intensity anomaly map overlayed over the sea chart over the area near Västervik in Sweden. As can be seen, the anomaly map has low resolution, and each pixel corresponds to an area of 185x185m^2. To estimate the magnetic field with greater accuracy, the map has been interpolated into the right part of Fig. 4, creating a high-resolution image. We then use nearby values for creating a PDF^{Magn} in a similar way as for creating the PDF^{Depth}.

C. Algorithm

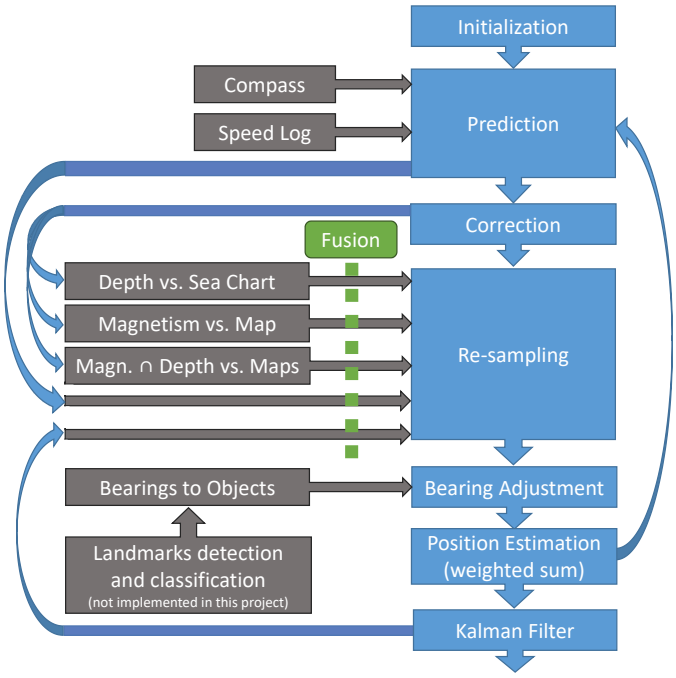

Fig. 5. The PF algorithm used in the project.

The specific PF algorithm used for this project is the Sampling Importance Resampling (SIR) [23], which we have slightly adjusted to enhance the robustness by fusion of various measurements. The high-level behavior (see Fig. 5) is as follows:

1) **Initialization** - Generate N particles and give them a random starting position around the initial starting position x_0 using (3).
2) **Prediction** - Move each particle according to the velocity vector measured by the compass and speed log, as well as an additional random velocity vector (see (4)).
3) **Correction** - Calculate weights for each particle given the maps and each particle's position. The weights are calculated for depth, magnetic field, and a combination of those two. Normalize the weights.
4) **Re-sampling** - The particles are resampled according to a distribution from subsets defined in Section III-D.
5) **Bearing Adjustment** - If a bearing to a landmark is detected, all particles that are outside a 2° corridor to the landmark are moved to a normal distribution around the bearing line.
6) **Iteration** Go to step 2.

To further enhance the performance, we used a KF for the final position estimation.

D. Fusion by Evaluating the Particles by Using Various Data

The Resampling Step creates particle subsets of defined sizes to benefit from the different available data. The weights created in the Correction Step can be based on either $Depth$, $Magnetic\ Intensity$, or the intersection $Depth \cap Magnetic\ Intensity$. We denote a PF that re-samples fully from only one of these subsets as PF^{Depth}, PF^{Magn}, or PF^{Comb}, and we denote a PF that re-samples from all the subsets as PF^{Fusion}. The particles can also just be dead reckoned using the compass and speed data (DR). The KF gives a good estimation of the correct location. Hence a small portion of the particles can be recreated at the KF estimation.

The subset sizes of the PF can be set arbitrarily, and we hypothesize that a well balanced PF^{Fusion} will perform better and especially be more robust compared to the other PFs using a single subset.

IV. System Setup

Our overarching goal is to provide insights from the evaluation of navigation tools for future affordable autonomous ships that can not rely on GNSS navigation alone due to safety constraints. The position accuracy gained when navigating is dependent on the performance of each navigation sensor. There are many possibilities to use better sensors, but these often come at a higher cost. A very expensive *Inertial Navigation Sensor* (INS) system can be used, which often has a drift of less than 1852m (1 Nautical Mile, NM) after 24h. In our previous work, we evaluated a PF using an INS like that, using simulated data [5]. A speed log that measures the *Speed Over Ground* (SOG) instead of *Speed Through Water* (STW) can also be used, as well as a *Multibeam Sonar* (MBE), which makes it possible to create an accurate 3D terrain of the bottom. These types of sensors have not been used for the presented work, as the high cost would limit the practical usage significantly.

Fig. 6. The boat of type CB90 used in the field trial.

We have based our algorithms and evaluations on the sensors used in the field trial, which we believe corresponds to

the setup of a typical future affordable autonomous ship. The boat used in this project is of type *CB90* (see Fig. 6), and has been complemented with some additional sensors to support the Swedish Universities via the WASP program [1] with a research platform for developing tools for autonomous ships. Data is collected from the digital compass onboard, but the ship is not equipped with a speed log. Instead, a virtual speed log has been created by using data from the GPS and adding an error of 0.2 knots (i.e., NM/h) (see Tab. I). In the last step, we add a drift (0.0 to 1.5 knots) to mimic the drift from the wind and current that can not be detected by the compass and speed log.

We mounted the magnetometer on the non-magnetic aluminum hull. Its purpose was to measure the anomalies of the magnetic intensity. As these anomalies are small, it is essential to know how the own ship disturbs the values when, e.g., a windshield wiper motor is started. During the data collection, this knowledge was not available, which unfortunately made the magnetic intensity values less accurate. The echo sounder system, on the other hand, was already installed and calibrated. Hence the data matched the sea chart well.

For obtaining the bearing information to landmarks detected in a video stream from a 360° camera, the intention was to mimic a system that would be able to detect, classify, and measure the bearings to visual landmarks. As we have not integrated this AI technology into our system yet, the bearings were measured manually from the video feed available on board.

Tab. I presents the data that we collected. We downsampled all the data to 0.5 Hz, as it was collected with a higher frame rate than needed. Also, the data from the GPS, which we used as ground truth, was downsampled to 0.5 Hz. With the used speed of the boat, 0.5 Hz implies that we get data every 9 m, which can be considered as relatively dense readings at sea. It should be pointed out that limitations of our approach are not due to limited sensor readings, as the bottleneck is the sparseness of information in the maps. In the right part of Fig. 3, it can be seen that there can be easily a distance of about 200 m between two bottom depth measurements in the sea chart.

TABLE I
SENSORS USED DURING FIELD TRIAL

Sensor	Description
Digital Compass*	Heading (Accuracy 0.5°) - 1Hz
Speed Log*	STW (Accuracy 1% + 0.1 knots) - 1Hz
Echosounder	Depth from surface to sea bed (Accuracy 0.1 m) - 1 Hz
Magnetometer	Magnetic Intensity measured as a vector - 100 Hz
360° camera	Provides visual image of the horizon around most of the ship. Can alternatively be multiple cameras. Images from 6 cameras were compiled into an image with a resolution of 16384x8192 - 15 Hz

*The digital compass and speed log could be exchanged to an INS.

The boat traveled a 17 km long route in the Swedish archipelago for 54 min. The route is shown in Fig. 3, where the weather conditions can be seen in one of the videos, accessed from one of the links, presented, e.g., in Fig. 7. We gathered 69 bearings to landmarks from the videos with at least a time of 30 s between each measurement.

V. TEST RUNS FOR EVALUATING AND OPTIMIZING THE POSITIONING ALGORITHM

We conducted a series of tests with various mixes of subsets used for the PFs. Every such subset mix is denoted as:

$$Depth\ A\%, Magn\ B\%, Comb\ C\%, DR\ D\%, KF\ E\% \quad (5)$$

This should be interpreted as A% of the particles are re-sampled using weights from the Correction Step created by comparing $Depth$ with the sea chart, B% from $Magnetic\ Intensity$, C% $Depth \cap Magnetic\ Intensity$, D% Dead Reckoned (DR), and E% from KF.

Each of the following tests is based on the same 54 min long data collection from the field trial, and has been conducted with a PF with 1000 particles. Different amounts of drifts have been added to stress test the algorithm. We present the main tests from this evaluation in Section V-C; however, we start out with presenting evaluations of tests for KF and DR.

A. Resampling from KF subset

In the following tests, we evaluate whether performance is improved by resampling 1% of the particles from the KF position estimation. We conducted a total of 12 tests, where half of the tests had a drift of 0.25 knots and the other half a drift of 0.75 knots. Various mixes were used according to Tab. II.

TABLE II
TEST USING KF POSITIONS

Drift	*Depth*	*Magn*	*Comb*	*DR*	*KF*	*Mean Pos Error (m)*
0.25	100	0	0	0	0	41.9
0.25	99	0	0	0	1	**37.5**
0.25	0	100	0	0	0	135.9
0.25	0	99	0	0	1	**130.6**
0.25	0	0	100	0	0	**85.6**
0.25	0	0	99	0	1	90.6
0.75	100	0	0	0	0	**92.9**
0.75	99	0	0	0	1	101.8
0.75	0	100	0	0	0	182.6
0.75	0	99	0	0	1	**176.1**
0.75	0	0	100	0	0	102.8
0.75	0	0	99	0	1	**99.5**

As can be seen in the table (the best value for each comparison is marked with bold text), the KF estimations seem to slightly improve the performance for most tests, especially for the tests having lower accuracy due to the weaker performance of the magnetic corrections. As we prioritize robustness, and we assume that the usage of the KF position will decrease our risk of starvation of particles at the correct location, we decide to use 1% KF for the rest of the tests.

B. Re-sampling from Dead Reckoned particles

In the following tests, we evaluated whether the performance is improved by each iteration randomly selecting 29% of the particles, and dead reckoning them instead of using the PF functionality. The benefit is that some particles will survive starvation during the specific iteration, even if the PF points the cloud in the wrong direction. The drawback is that the performance of the DR will decrease as the drift increases. We conducted a total of 12 tests, where half of the tests had a drift of 0.25 knots and the other half a drift of 0.75 knots. We used various mixes according to Tab. III.

TABLE III
TEST USING DR

Drift	*Depth*	*Magn*	*Comb*	*DR*	*KF*	*Mean Pos Error (m)*
0.25	99	0	0	0	1	**37.5**
0.25	70	0	0	29	1	42.6
0.25	0	99	0	0	1	130.6
0.25	0	70	0	29	1	**124.2**
0.25	0	0	99	0	1	90.9
0.25	0	0	70	29	1	**73.9**
0.75	99	0	0	0	1	**101.8**
0.75	70	0	0	0	1	197.0
0.75	0	99	0	0	1	**176.1**
0.75	0	70	0	0	1	194.8
0.75	0	0	99	0	1	**99.5**
0.75	0	0	70	0	1	100.5

The results were somewhat ambiguous, as only 2 tests out of 6 indicated that the performance increased by using DR. Our main comparison, presented in Fig. 9, will, by this, compare the PF^{Fusion} to mixes with both 29% DR and 0% DR.

C. Fusion of Sensor Data to Increase the Robustness of the PF

We assume that the depth measurements are more valuable compared to magnetic intensity when it is possible to keep track of the position accurately. This is due to the magnetic intensity sensor being less accurate, and these maps being more diffuse and of lower resolution than the sea chart. As the position estimation worsens, e.g., due to higher drift or outliers, we predict the magnetic intensity to increase in value. When depth and magnetic intensity give similar position accuracy, the combination (intersection) probably gives higher accuracy than each of them individually.

The challenge when having low accuracy is that a PF corrected by one type of data easily suffers from sample impoverishment when some outliers impair the calculations. By letting some of the particles be dead reckoned, and some particles regenerated from the KF position estimation (in our case set to 1%), we suspect the robustness to increase.

After a structured series of tests that we based on these assumptions, where we, e.g., assumed $Depth$ to be more valuable than $Magnetic\ Intensity$, we have found that (6) expresses a well-balanced mix for PF^{Fusion}.

$$Depth\ 40\%, Magn\ 15\%, Comb\ 25\%, DR\ 19\%, KF\ 1\% \quad (6)$$

The tests were conducted using various amount of drift to find a mix that could perform well during various conditions. We will use this mix as a reference throughout the following evaluations of the PF performance.

For these tests, we used various mixes for the re-sampling step while having a various amount of drift. PF^{Depth}, PF^{Magn}, PF^{Comb}, and PF^{Fusion} were compared while having 0.0 to 1.5 knots of drift. The simulations were made using both 29% DR and 0% DR for PF^{Depth}, PF^{Magn}, and PF^{Comb}, giving a total of 49 tests.

Fig. 7 shows four of these 49 tests, where we have used 0.25 knots drift speed and 29% DR. For this modest drift, PF^{Depth} performs best, PF^{Fusion} next best, PF^{Comb} a little worse, and PF^{Magn} the worst, due to the lower accuracy of the magnetic map and sensor.

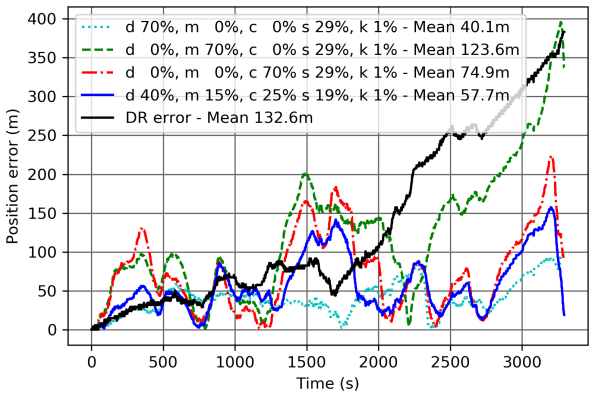

Fig. 7. PF^{Depth} gives the best performance when having 0.25 knots driftspeed. PF^{Fusion} gives the next best performance. (See videos on https://youtu.be/5wXou74isso.)

When having a higher drift speed, see Fig. 8, both PF^{Depth} and PF^{Comb} lose track of the position, which results in poor performance. In these prerequisites, PF^{Fusion} has the best performance.

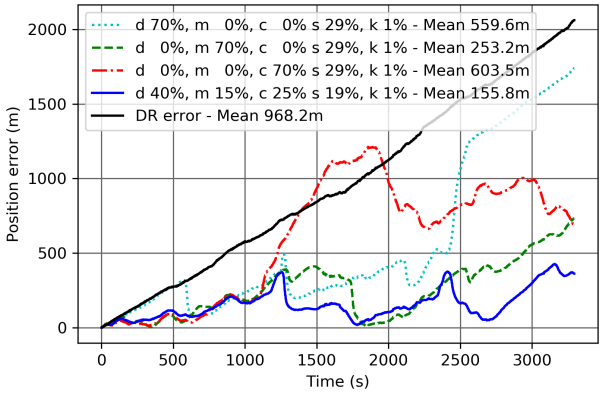

Fig. 8. When having 1.25 knots driftspeed, PF^{Fusion} gave the best performance. (See videos on https://youtu.be/ELi7ALXImm4.)

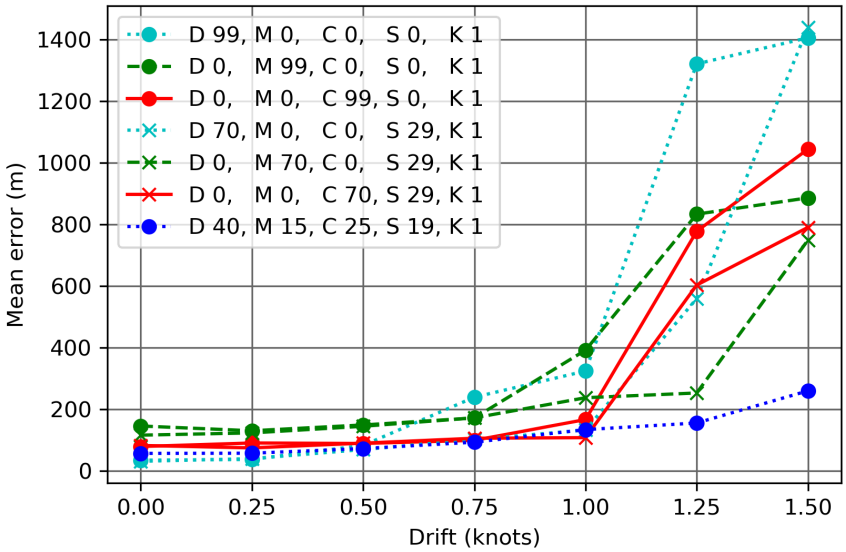

Fig. 9. The diagram shows the results from 49 simulations when using various mixes during various drift speeds. The PF which re-samples from multiple subsets (PF^{Fusion}) has the best robustness, and performs well during all drift speeds. It has a good accuracy for all drift speeds.

We show all 7x7 test results in Fig. 9. The data shows that PF^{Depth} performs well when there is a slow drift, but as the drift increases and the position estimation diverges from the correct location, the performance of the PF^{Depth} quickly weakens. The PF^{Fusion}, on the other hand, has quite good performance over all evaluated drift speeds.

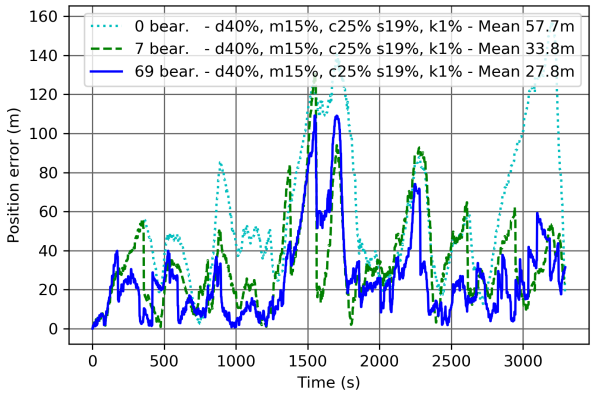

Fig. 10. Tests that show how bearings to landmarks can reduce the position error when having a low drift and using the PF^{Fusion}. (See videos on https://youtu.be/8nHf7cuIyGA.)

D. Using landmarks to increase the performance and robustness

If the ship is equipped with a system that can detect bearings to known landmarks, these can be used to adjust the particles' positions. In the tests presented in Fig. 10, we evaluate how the performance improves by the usage of bearings. We have set the drift speed to 0.25 knots. In the first test, we use no bearings to landmarks. In the second test, we use 7, which results in a substantial performance gain. In the last test, 69 bearings are used, which increases the performance slightly more. As can be seen in the linked video, the particles are continually adjusting to the bearings, thereby maintaining the position accuracy. By at least occasionally updating the particle position from bearings, the risk of particle starvation at the correct position is lowered.

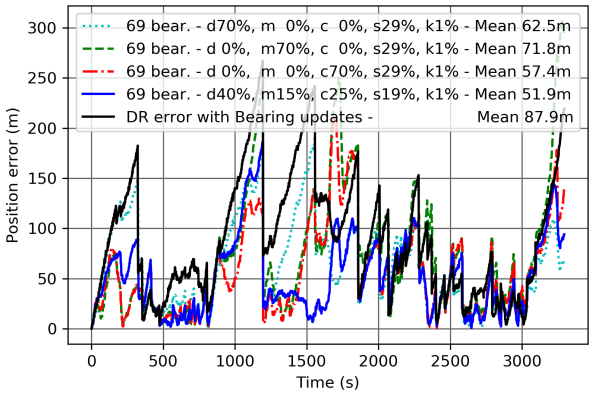

Fig. 11. Tests that show that the fusion mix outperform the other mixes while having the high drift speed 1.5 knots, and using all 69 bearings. (See videos on https://youtu.be/ZJG-CyMcWpI.)

In Fig. 11, we present tests with a higher drift, where we compare different mixes where the particles are updated from all the 69 bearing updates. As can be seen, the PF^{Fusion} performs best also in these tests.

VI. Conclusion

Other research has already shown that PFs can be used for position estimations when a high-resolution 3D terrain map is available. In our study, we have a broader use-case where we instead use publicly available maps, such as sea charts. We have shown that low-accuracy maps can be used, and more importantly, we have shown that by fusing measurement evaluations based on several such low-accuracy maps, the robustness of the system can be increased. In our study, we have used an increased position drift as a stress-test for our algorithm. Nevertheless, it should be noted that the algorithm will also be more resilient to outliers in sensor measurements or map accuracy, to flat terrains, and symmetric terrains, as long as these difficulties do not arise in all domains at the same time.

Humans mostly use GNSS systems as the primary way of determining the position but are also monitoring terrestrial navigation as a redundancy. We propose that autonomous ships could use GNSS systems, but for safety reasons also should cross-reference with a system such as a TAN with multiple data sources. All this can be achieved with affordable sensors, which we have used in this work. Our future efforts are targeting the integration of our positioning approach into an earlier presented VR based visualization and control tool for remote supervision of (semi-)autonomous vessels [3]. We also plan to develop an ML-based tool for evaluation of the current seabed and magnetic field anomaly map. This evaluation data will then be used by the algorithm to dynamically adjust the subset sizes of PF^{Fusion} to optimize the performance even further.

References

[1] (2020) WASP. Last accessed 29 January 2020. [Online]. Available: http://wasp-sweden.org/

[2] T. E. Humphreys, B. M. Ledvina, M. L. Psiaki, B. W. O'Hanlon, and P. M. Kintner, "Assessing the spoofing threat: Development of a portable GPS civilian spoofer," in *Radionavigation Laboratory Conference Proceedings*, 2008.

[3] M. Lager and E. A. Topp, "Remote supervision of an autonomous surface vehicle using virtual reality," *IFAC-PapersOnLine*, vol. 52, no. 8, pp. 387–392, 2019.

[4] S. R. Chan, N. A. Hamid, and K. Mokhtar, "A theoretical review of human error in maritime accidents," *Advanced Science Letters*, vol. 22, no. 9, pp. 2109–2112, 2016.

[5] M. Lager, E. A. Topp, and J. Malec, "Underwater terrain navigation during realistic scenarios," in *Multisensor Fusion and Integration for Intelligent Systems*. Springer, 2017, pp. 186–209.

[6] N. Merlinge, J. Brusey, N. Horri, K. Dahia, and H. Piet-Lahanier, "Enhanced cooperative navigation by data fusion from imu, ambiguous terrain navigation, and coarse relative states," in *2017 IEEE 56th Annual Conference on Decision and Control (CDC)*. IEEE, 2017, pp. 375–380.

[7] S. Carreno, P. Wilson, P. Ridao, and Y. Petillot, "A survey on terrain based navigation for auvs," in *OCEANS 2010*. IEEE, 2010, pp. 1–7.

[8] R. Karlsson and F. Gustafsson, "Bayesian surface and underwater navigation," *IEEE Transactions on Signal Processing*, vol. 54, no. 11, pp. 4204–4213, 2006.

[9] D. Peng, T. Zhou, J. Folkesson, and C. Xu, "Robust particle filter based on huber function for underwater terrain-aided navigation," *IET Radar, Sonar & Navigation*, vol. 13, no. 11, pp. 1867–1875, 2019.

[10] G. T. Donovan, "Position error correction for an autonomous underwater vehicle inertial navigation system (ins) using a particle filter," *IEEE Journal of Oceanic Engineering*, vol. 37, no. 3, pp. 431–445, 2012.

[11] T. Nakatani, T. Ura, T. Sakamaki, and J. Kojima, "Terrain based localization for pinpoint observation of deep seafloors," in *OCEANS 2009-EUROPE*. IEEE, 2009, pp. 1–6.

[12] N. Fairfield and D. Wettergreen, "Active localization on the ocean floor with multibeam sonar," in *OCEANS 2008*. IEEE, 2008, pp. 1–10.

[13] K. B. Anonsen and O. Hallingstad, "Terrain aided underwater navigation using point mass and particle filters," in *Position, location, and navigation symposium, 2006 IEEE/ION*. IEEE, 2006, pp. 1027–1035.

[14] F. C. Teixeira, J. Quintas, P. Maurya, and A. Pascoal, "Robust particle filter formulations with application to terrain-aided navigation," *International Journal of Adaptive Control and Signal Processing*, vol. 31, no. 4, pp. 608–651, 2017.

[15] M. Zhou, R. Bachmayer, and B. deYoung, "Working towards adaptive sensing for terrain-aided navigation," in *2019 International Conference on Robotics and Automation (ICRA)*. IEEE, 2019, pp. 3450–3456.

[16] G. Salavasidis, A. Munafò, C. A. Harris, T. Prampart, R. Templeton, M. Smart, D. T. Roper, M. Pebody, S. D. McPhail, E. Rogers *et al.*, "Terrain-aided navigation for long-endurance and deep-rated autonomous underwater vehicles," *Journal of Field Robotics*, vol. 36, no. 2, pp. 447–474, 2019.

[17] I. Nygren, "Terrain navigation for underwater vehicles," Ph.D. dissertation, KTH, 2005.

[18] S. Dektor and S. Rock, "Improving robustness of terrain-relative navigation for auvs in regions with flat terrain," in *2012 IEEE/OES Autonomous Underwater Vehicles (AUV)*. IEEE, 2012, pp. 1–7.

[19] ——, "Robust adaptive terrain-relative navigation," in *Oceans - St. John's*. IEEE, 2014, pp. 1–10.

[20] E. Le Grand and S. Thrun, "3-axis magnetic field mapping and fusion for indoor localization," in *2012 IEEE International Conference on Multisensor Fusion and Integration for Intelligent Systems (MFI)*. IEEE, 2012, pp. 358–364.

[21] M. Frassl, M. Angermann, M. Lichtenstern, P. Robertson, B. J. Julian, and M. Doniec, "Magnetic maps of indoor environments for precise localization of legged and non-legged locomotion," in *2013 IEEE/RSJ International Conference on Intelligent Robots and Systems*. IEEE, 2013, pp. 913–920.

[22] C. Musso, A. Bresson, Y. Bidel, N. Zahzam, K. Dahia, J.-M. Allard, and B. Sacleux, "Absolute gravimeter for terrain-aided navigation," in *2017 20th International Conference on Information Fusion (Fusion)*. IEEE, 2017, pp. 1–7.

[23] F. Gustafsson, "Particle filter theory and practice with positioning applications," *IEEE Aerospace and Electronic Systems Magazine*, vol. 25, no. 7, pp. 53–82, 2010.